Drop Impact and Agglomeration Under Static Powder Bed Conditions

Andrew C. S. Lee and Paul E. Sojka
Maurice J. Zucrow Laboratories, School of Mechanical Engineering, Purdue University, West Lafayette, IN 47907

DOI 10.1002/aic.12575
Published online April 11, 2011 in Wiley Online Library (wileyonlinelibrary.com).

The influence of impact conditions (reported in terms of Weber and Reynolds numbers) on nucleus formation was studied for single drops striking a static glass bead bed. Results from high speed images showed that the nucleation rate is not influenced by liquid physical properties (density, surface tension, viscosity) for drops that spread significantly ($30 < We < 233$). Results also showed that nucleus size is determined by how much liquid penetrates into the bed during drop spreading, so does depend on surface tension and liquid density. A corresponding analytical model, derived from first principles, predicts nucleus size to with 1.5% using only liquid physical and powder bed properties, plus the experimentally measured drop spreading behavior. © 2011 American Institute of Chemical Engineers *AIChE J,* 58: 79–86, 2012
Keywords: wet granulation, nucleation, drop impact, wetting, spreading

Introduction

Interactions between the liquid and powder inside a granulator are very complex. Over the years, researchers have identified several key processes that influence granulating behavior: (1) wetting and nucleation, (2) consolidation and growth, and (3) attrition and breakage.[1,2] This investigation is concerned with initial interactions (impact and spreading) between discrete liquid drops and powder bed surface as part of a comprehensive wetting and nucleation study.

Drop impact on a deformable surface such as a powder bed has not been studied widely. This is partly because rearrangement of particles at the impact site introduces complications when describing the spreading behavior of the impacting drop. As examples, drops impacting a powder bed show spreading, receding, and splashing behavior similar to those impacting a flat surface.[3]

On a powder bed there are additional phenomena, one being a drop absorbing particles it is in contact with. This drop-particle combination is called a nucleus and it becomes the core of any agglomerate(s). Our focus is on how the drop impact process influences the rate of nuclei formation and nuclei size.

There is limited work on drop impact on a powder bed, despite the fact that it is an unavoidable part of nucleation. Agland and Iveson[3] conducted experiments where dyed drops were directed onto a glass bead bed. The impact velocity was varied and behavior recorded at up to 400 frames per second (fps). Their observations are summarized in Figure 1. Due to the low temporal resolution of their camera the time evolution of drop shape could not be determined.

Hapgood[4] performed experiments similar to those of Agland and Iveson,[3] but using a polymeric solution and lactose. While her 30 fps camera could not provide time resolved information, she contended that the impact crater was significantly deeper than observed by Agland and Iveson with the difference ascribed to the methods used to produce the beds. Agland and Iveson fluidized their glass beads and then decreased the air velocity slowly to settle them down. Hapgood poured lactose onto a Petri dish and scraped off the top layer. Hapgood's work therefore suggests that liquid drop-surface interactions are influenced by material packing characteristics.

In more recent experiments, Eshtiaghi et al.[5] observed that drops impacting beds of hydrophobic powders at higher velocities produced liquid marbles of higher powder content.

Correspondence concerning this article should be addressed to A. C. S. Lee at leeac@purdue.edu.

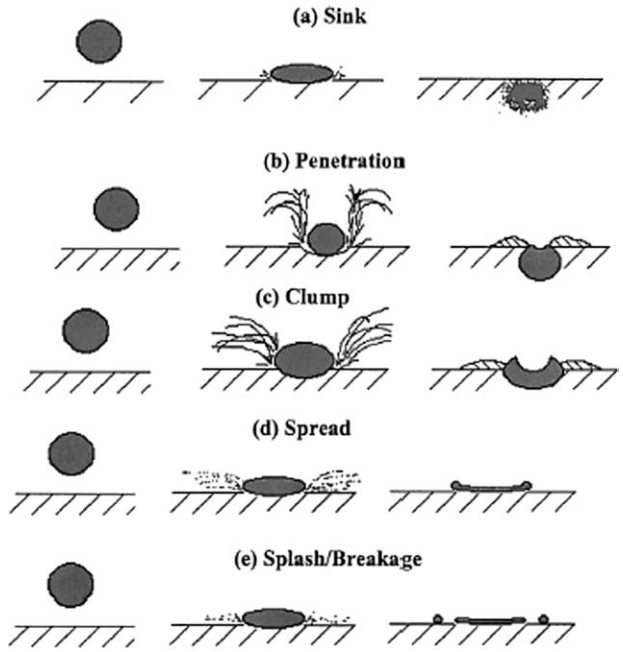

Figure 1. Outcomes of drop impact on a powder bed (adopted from Agland and Iveson[3], time progression is to the right, impact velocity increases downward.

They suggest that drops with higher velocities can spread more upon impact and make contact with more particles, which would result in an increased amount of powder on the drop surface when it recoils.

In many nucleation studies, granules were sampled in the middle of the operation, or at a significant time (on the order of seconds to minutes) after liquid-powder bed contact.[6–10] Furthermore, the sampled granules were mostly dried before any analysis. With these types of sampling schemes, it was not only difficult to investigate the initial liquid drop-powder bed interaction, but was also almost impossible to deconvolute the effect of nucleation from other liquid-solid interactions.[2,11]

Very little information is available in the literature regarding the nucleation kinetics (e.g., time it takes to form a granule, or the temporal dependence of the nuclei size). Rather, several researchers have used an analytical expression for the time it takes a drop to completely penetrate a powder bed as a scale for estimating nucleation rate.[9,10,12–14] One of the most widely used was proposed by Hapgood et al.[14] after adopting drop penetration models from Denesuk et al.[15] and Middleman[16]:

$$t_{\text{pen}} = 1.35 \frac{V_0^{2/3}}{\varepsilon_{\text{eff}}^2 R_{\text{eff}}} \frac{\mu}{\sigma \cos\theta} \tag{1}$$

Here V_0 is the initial drop volume, μ the liquid viscosity, σ the surface tension, θ the contact angle, ε_{eff} the effective powder bed porosity, and R_{eff} the effective pore radius. Key assumptions underlying Eq. 1 are: (1) the contact area between the drop and the porous surface is constant throughout the entire penetration process and (2) the contact radius is the same as the radius of the liquid drop before contact. It will be shown in a later section that the contact area and radius can vary significantly during the impact and penetration processes, and that they are strongly influenced by the impact condition and liquid properties. These assumptions limit agreement between predictions using Eq. 1 and experimental data to approximately an order of magnitude.

Based on the limitations outlined above, the objectives of this study were twofold. First, to gain better insight into the temporal evolution of a drop impacting a static powder bed, and the subsequent nucleation process. Second, to develop an analytical model that predicts the size of nuclei formed using only the spreading characteristics of the drop and the material properties of the liquid and particles.

Experimental Setup

The experimental setup used in this study is similar to that of Agland and Iveson[3] and is depicted in Figure 2. Agglomerates were formed by releasing drops of water, a polymer-water mixture, or a glycerin-water mixture above a bed of glass beads. The liquid physical properties are listed in Table 1 along with their experimental uncertainties.

Drops were produced by forcing the liquids slowly through a 0.15 mm ID/0.30 mm OD hypodermic needle. Drop size was estimated using $D_0 = (6d\sigma/\rho g)^{1/3}$, where d is the OD of the hypodermic needle, σ the interfacial tension, ρ the liquid density, and g the gravitational acceleration. Discrepancies between the estimated and measured D_0 values were within 3%, with all drops between 2.1 and 2.4 mm in diameter.

The powder bed was prepared by overfilling a Petri dish with glass spheres (representing spherical, nonporous particles) and scraping off the excess material with a straight edge. The particle size distribution was measured using a Mastersizer 2000 mated with a Hydro 2000S wet sample dispersion unit, both from Malvern Instruments, Ltd. The particle size range was ~160 to 300 μm, while the Sauter mean

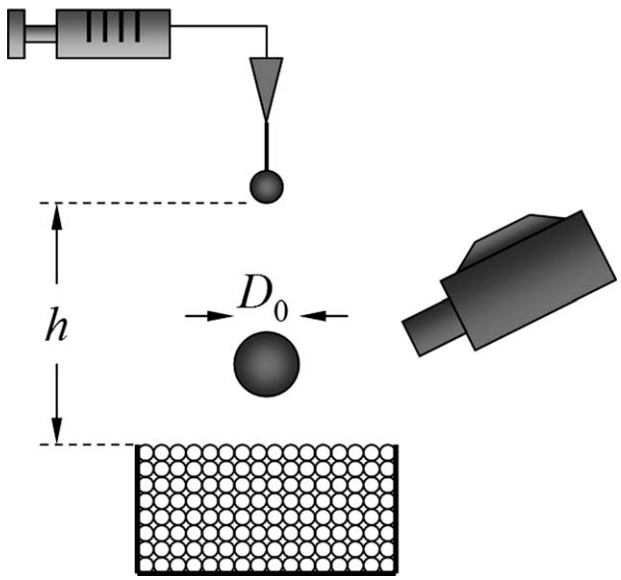

Figure 2. Experimental setup.

Table 1. Physical Properties of Liquids at 20°C

Liquid	D_0 (mm)	ρ (kg/m^3)	$\mu\cdot\times 10^3$ [kg/(m s)]	$\sigma\cdot\times 10^3$ (kg/s^2)	θ (°)
Distilled water	2.37	991 ± 6	1.101[b]	71.9 ± 0.1	17.9 ± 1.9
95% glycerin[a]	2.12	1239 ± 7	544 ± 25	64.7 ± 0.1	31.0 ± 3.0
85% glycerin[a]	2.14	1210 ± 7	125 ± 3	65.6 ± 0.0	21.3 ± 5.2
60% glycerin[a]	2.16	1147 ± 8	13 ± 1	63.4 ± 0.3	22.5 ± 2.6

[a]All solutions are water-based and solution concentration is by weight.
[b]Fox et al.[17]

diameter (D_{32}) was 213 μm. The drop size-to-particle size ratio (i.e., D_0/D_p) was therefore ~10. As a result, one expects immersion type nucleation where a drop engulfs smaller particles, as proposed by Schaefer and Mathiesen.[18]

The powder bed porosity was calculated using $\varepsilon = 1-(\rho_{bulk}/\rho_{true})$ where ρ_{bulk} is the poured density and ρ_{true} the true density of glass beads. ρ_{bulk} was measured to be 1.39 ± 0.04 g/mL using a graduated cylinder and digital scale. ρ_{true} was taken as the nominal glass density, 2.50 g/mL, which resulted in $\varepsilon = 0.44 \pm 0.02$.

When the drop impacts the powder bed, the region under the impacting drop is likely to be compressed and one would expect to see a change in ε. However, in a powder bed of nonporous, rigid, and spherical particles with narrow size distribution, such as that used in the current study, any change in ε due to compression of the bed is expected to be low. In fact, when ρ_{bulk} was being measured, the graduated cylinder was tapped against a table one to five times to check the change in ρ_{bulk} and the resulting ε, but the variations were smaller than the experimental uncertainties mentioned above. Therefore, the porosity is assumed to remain nearly constant during the impact process.

The bed effective pore diameter, R_{por}, was calculated using the Kozeny equation:

$$R_{por} = \frac{D_p}{3}\frac{\varepsilon}{(1-\varepsilon)} \quad (2)$$

Substituting D_{32} for D_p gives $R_{por} = 55.8$ μm.

The drop impact velocity was varied by altering the release height for $0.4 \le H \le 30$ cm. For this range of H, the impact velocity was estimated using $U = \sqrt{2gH}$. The agreement between the computed and directly measured impact velocities (using a high speed video camera) was within experimental uncertainties associated with the direct measurement, which were at most 10%, and less than 2% for $H > 5$ cm.

Based on the physical properties of the liquids and the impact velocities, the range of impact Weber number ($We = \rho U^2 D_0/\sigma$) in the current study was $5 \le We \le 233$, and that for impact Reynolds number ($Re = \rho U D_0/\mu$) was $2 \le Re \le 5112$.

Drop impact, spreading, and nucleation were captured using a Phantom v7.1 high speed digital video camera from Vision Research Inc. The camera was mated to an AF Micro-Nikkor 105 mm f/2.8 close-up lens. Captured video images were played back using Vision Research Inc. video software. The highest frame rate used in this study was 5000 fps.

Illumination was provided by a 200 W halogen lamp. Due to the amount of heat generated by the lamp, it was only on when the high speed video camera was sampling, (i.e., for 2–5 s at a time) and with at least 3 minutes of cooling period between runs.

Experimental Results: Measurement of Nuclei Sizes

No splashing upon impact was observed for the range of *We* considered here. However, two distinct behaviors were observed depending on *We*.

When $We \le 13$, the drop landed on the powder bed surface without noticeably disturbing the landing site. See Figure 3. After impact, the drop oscillated for a time before attaining a spherical cap shape. Initial oscillation appeared similar for all drops, but duration increased with rising liquid viscosity (~18 ms for distilled water and 50 ms for 2.5% HPMC). All drops penetrated the powder bed without a noticeable change in their base diameter, which is similar to the constant drawing area pattern described by Denesuk et al.[15] The penetration time was longer for a more viscous liquid, as predicted by Eq. 1. After most of the visible volume of the drop had penetrated into the bed, all drops left a slight berm around the penetration site, which was circular when viewed from above.

When *We* was increased to 30, the drop spread and made a significant impact crater. The initial spreading was completed within 1.6–2.0 ms after impact, regardless of *We* or *Re*. Drops recoiled after reaching their maximum spread. During recoil, glass beads that were in contact with the drop were separated from the rest of the bed and incorporated into the drop to form a more or less spherical nucleus. Figures 4 and 5 show this process for different liquid drops released from $H = 10$ cm ($62 \le We \le 76$) and $H = 30$ cm

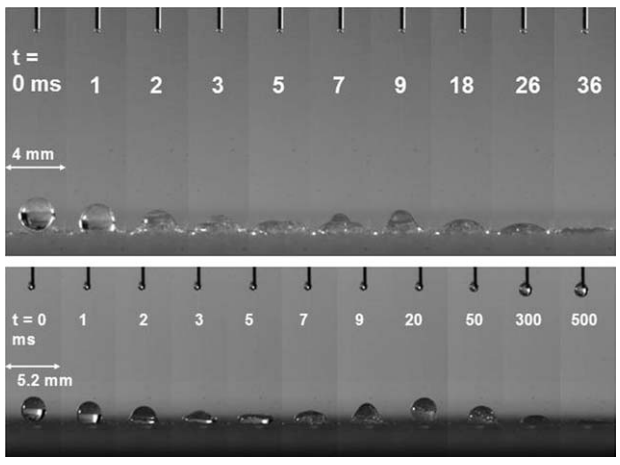

Figure 3. Impact and penetration behavior of distilled water drop (top) and 2.5% HPMC solution drop (bottom); *H* = 2.0 cm for distilled water (*We* = 10, *Re* = 1166) and *H* = 1.3 cm for 2.5% HPMC (*We* = 9, *Re* = 20).

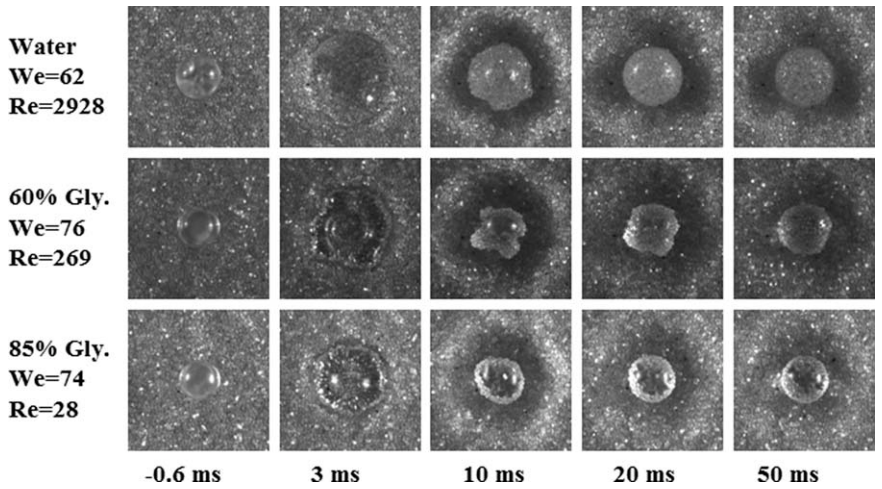

Figure 4. Impact and nucleation behavior for various liquid drops falling from $H = 10$ cm.

($218 \leq We \leq 233$), respectively. Recoiling was complete by 20 to 30 ms after impact, although minor oscillation of the nucleus continued for a few additional milliseconds. By 50 ms after impact, clearly visible nuclei were formed at the bed surface regardless of the release height or liquid type.

Figure 6 shows the dimensionless spreading diameter of the drop base, $D_b(t)/D_0$, as a function of time after impact for selected cases. The spreading pattern was initially circular, but started to form fingers as it neared its maximum. Therefore, $D_b(t)$ was estimated by measuring the maximum semimajor axis of the spreading drop.

After a nucleus initially attained its spherical shape, the liquid inside slowly drained into the bed. This caused the nucleus to deform. The drainage rate was different for different liquids, and it could take from several seconds to hours before drainage stopped depending on liquid type. This secondary phenomenon is not a focus of the current study so will not be discussed here.

The key factor in nucleation behavior at $We \geq 30$ is the impact force of the drop. At lower We, a drop does not overcome its interfacial tension force so it does not spread significantly beyond its initial diameter. As result, it quickly reaches a spherical cap shape and sits on the bed surface. At higher We, a drop spreads and causes deformation at the landing site. The spread drop recoils because of interfacial tension and forms a liquid-particle mixture, a nucleus, as the particles that were in contact with the spreading drop are pulled into it as it retracts.

Nuclei sizes were measured and plotted against impact Weber number and impact Reynolds number in Figures 7 and 8, respectively, to study the influence of impact conditions on nucleation. All nuclei sizes were measured 50 ms after impact. This time was chosen because all liquid drops, except those of distilled water, produced spherical nuclei by this time (The drainage rate was so fast for distilled water that there was no sensible period of time during which the nucleus shape or size remained constant. Also, some distilled water drops were not able to retract into a spherical shape because of rapid penetration. Therefore, nuclei formed from distilled water are not included in the following discussions). Nuclei sizes were measured by counting pixels in both the horizontal and vertical directions and by

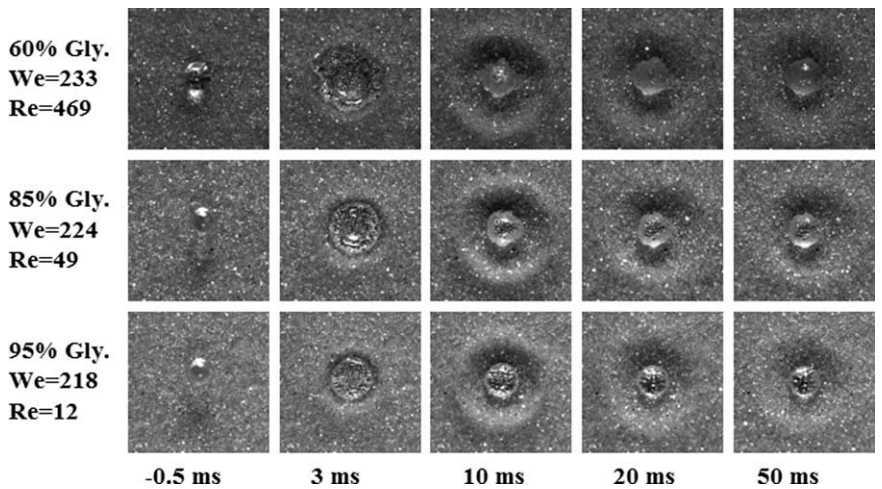

Figure 5. Impact and nucleation behavior for various liquid drops falling from $H = 30$ cm.

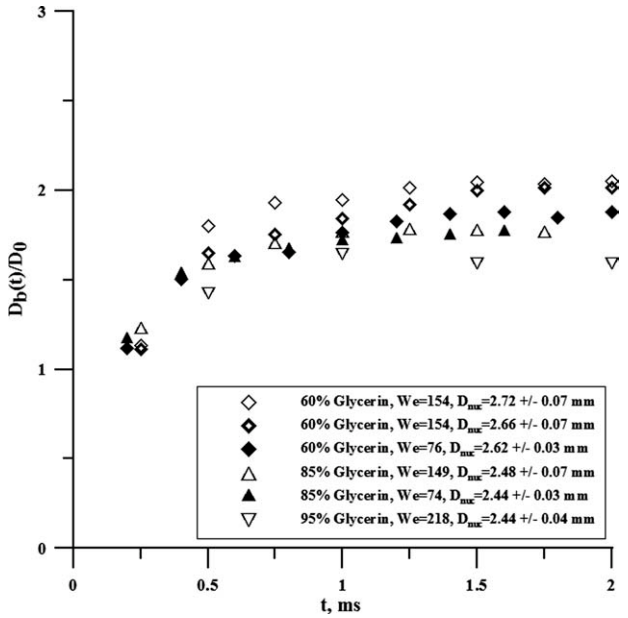

Figure 6. Early impacting drop evolution; D_{nuc} were measured 50 ms after the impact; uncertainty bars are equal to or smaller than the symbol size.

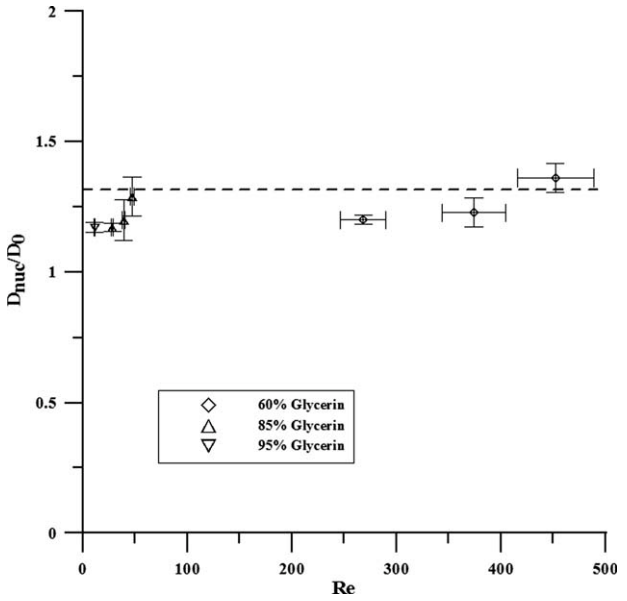

Figure 8. Nucleus size versus impact Reynolds number; same experimental conditions as in Figure 7.

The dashed line represents the theoretical value for $D_{nuc,max}/D_0$.

taking the arithmetic mean. Each data point is an average of three separate trials. The vertical uncertainty bars represent one standard deviation. The horizontal uncertainty bars indicate uncertainties associated with estimation of *We* and *Re*. The horizontal dashed lines shown in the figures are the maximum theoretical nucleus size, which will be discussed in the next section.

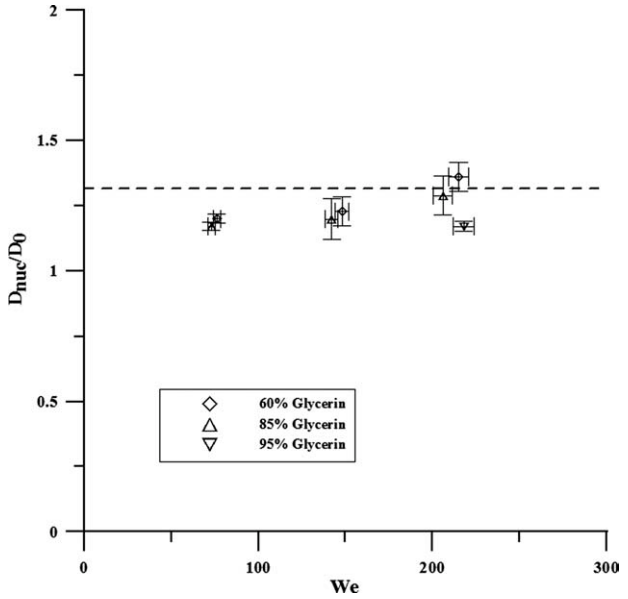

Figure 7. Nucleus size versus impact Weber number; all D_{nuc} were measured 50 ms after the impact.

The dashed line represents the theoretical value for $D_{nuc,max}/D_0$.

Both Figures 7 and 8 show weak dependences of D_{nuc}/D_0 on *We* or *Re*. However, they do show that D_{nuc}/D_0 is roughly 1.2 regardless of *We* or *Re*. In the studies by Schaafsma et al.[7] and Waldie,[8] where granules were produced using setups similar to this one, the granule-to-drop size ratio ranged from 1.5 to 2.6. The main difference was the sampling time. Drops were allowed more time in the powder bed before being sampled in the works of Schaafsma et al. and Waldie.[8]

Model: Prediction of Nuclei Sizes

An analytical model to predict the size of nuclei formed via the behavior observed was developed for $30 \leq We \leq 233$. The idealized process illustrated in Figure 9 was adopted.

Immediately following impact, a drop spreads radially as well as into the powder bed. It is not known exactly how the drop boundary propagates into the bed so we assume the profile is hemispherical. During this time, the liquid is in contact with the powder bed beneath it and starts to penetrate due to capillary action. After the drop has spread to its maximum extent, it recedes and carries along with it particles that it contacted. In the video it was observed that impact craters continue to open even after drops start to recoil. When the layer of particles under the drop separates from the rest of the bed, the drop does not ''see'' any more pores to penetrate. Thus, it is assumed that penetration stops at maximum spreading. Finally, a nucleus is formed as the liquid-particle mixture contracts to a sphere. There was no visible splashing of the impacting drop under current experimental conditions.

One of the most common descriptions of a nucleus is its high moisture level, meaning that most of the interstitial voids are filled with liquid. Assuming no splashing and no air inside a nucleus, the volume V_{nuc} is equal to the sum of the initial

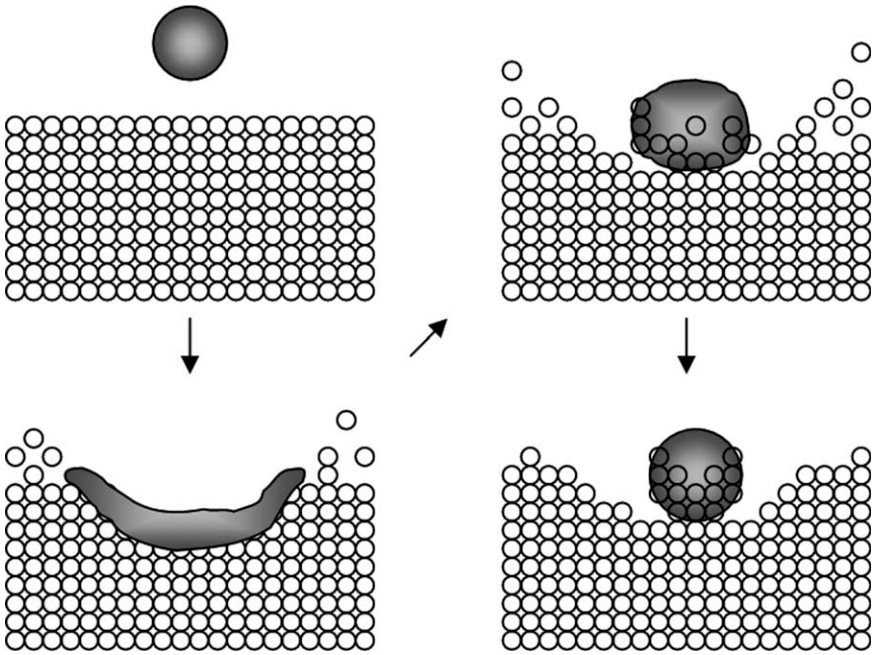

Figure 9. Formation of nucleus immediately following drop impact.

drop volume V_0 and the total volume of particles that make contact with the drop, V_S, i.e., $V_{nuc} = V_0 + V_S$. With all interstitial voids in the nucleus filled with liquid, V_S is equal to $V_{pen}\cdot[(1-\varepsilon)/\varepsilon]$, where V_{pen} is the amount of liquid that penetrates into the bed during spreading and ε is the void fraction, or porosity, of the bed. The sphere equivalent diameter of a nucleus is:

$$D_{nuc} = \sqrt[3]{\frac{6}{\pi}\left(V_0 + V_{pen}\left(\frac{1-\varepsilon}{\varepsilon}\right)\right)} \tag{3}$$

D_{nuc} reaches a maximum when the entire volume of drop penetrates the bed during spreading and the liquid-particle mixture contracts to a sphere. The maximum D_{nuc} is equal to $\sqrt[3]{6/\pi(V_0/\varepsilon)}$, or $D_0/\varepsilon^{1/3}$. Therefore, the dashed lines shown in Figures 7 and 8 represent the value $D_{nuc,max}/D_0 = 1/\varepsilon^{1/3}$ (or $D_{nuc,max}/D_0 \approx 1.31$).

In reality, liquid drops are not able to contract to spheres if the solids content is too high. This causes overestimation of D_{nuc}, which was more often seen in less viscous liquids such as distilled water and 60% glycerin.

V_{pen} is time dependent because (1) the contact area between the drop and bed changes during spreading and retraction and (2) the rate of liquid penetration is different for different liquids. The longer the time of contact, or the larger the contact area, the more liquid will penetrate into the bed. Also, any reduction in the resistance to liquid penetration, such as the viscous force, will increase the rate of liquid penetration. This behavior can be observed when a volume of liquid is in contact with a bundle of capillaries.

An expression to predict V_{pen} is now developed by assuming the powder bed acts as a bundle of capillaries (Figure 10). It is based on the Washburn[19] model for liquid flow in a cylindrical capillary.

Imagine a viscous liquid flowing through a cylinder having a constant radius, R_{por}. Assuming (1) the flow is laminar, (2) gravitational effects are small compared to viscous effects, and (3) the capillary is completely wetted by the liquid, the Navier-Stokes equations reduce to the Hagen-Poiseuille form:

$$u_{avg} = \frac{dh_{pen}}{dt} = \frac{1}{8\mu}\frac{\Delta P}{h_{pen}}R_{por}^2 \tag{4}$$

Here, u_{avg} is the average velocity of the liquid, h_{pen} and R_{por} are the length of the liquid column in the capillary and its radius, respectively, μ is the liquid viscosity, and ΔP is the pressure differential driving the flow. Washburn suggested that there are three major components to ΔP: (1) hydrostatic head, (2) resistance due to air flow in the capillary as it is replaced by the liquid, and (3) capillary pressure due to surface tension. Assuming the capillary pressure is the dominant factor, Eq. 4 can be rearranged and integrated to yield one of several variants:

$$h_{pen}(t) = \sqrt{\frac{\sigma\cos\theta R_{por}}{2\mu}t} \tag{5}$$

The differential volume of liquid that is in the capillaries, dV_{pen}, is:

$$dV_{pen} = \left(\pi R_{por}^2 dh_{pen}\right)\left(\rho_{por}^* \frac{8}{2}\pi r dr\right) \tag{6}$$

where ρ_{por}^* is the number density of capillary entrances in a given surface area. This is the approach Denesuk et al.[15] used, except they employed a planar liquid spreading profile whereas a hemispherical one is used here.

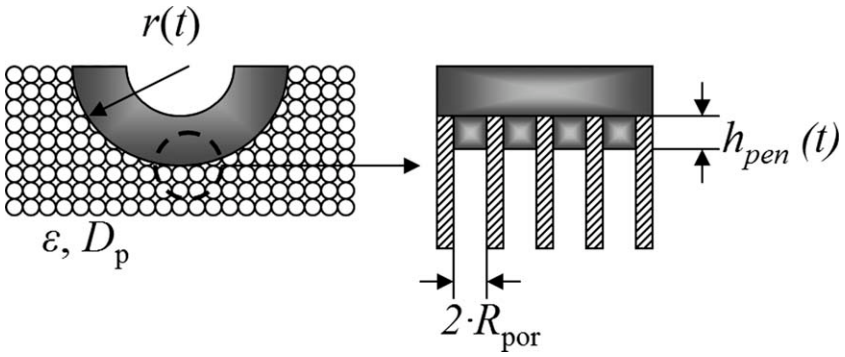

Figure 10. Powder bed beneath the liquid modeled as a bundle of capillaries of equal diameters (right). Spreading profile of of the impacting drop is assumed to be spherical (left).

The expression in the first parentheses on the right hand side of Eq. 6 is the volume of liquid in a single capillary. The one in the second parentheses is the total number of capillaries in contact with the liquid. dh_{pen} can be obtained by differentiating Eq. 5 with respect to t. Substituting it into Eq. 6 gives:

$$dV_{\mathrm{pen}} = \left(\pi R_{\mathrm{por}}^2 \rho_{\mathrm{por}}^*\right)\left(2\pi\sqrt{\frac{\sigma\cos\theta R_{\mathrm{por}}}{2\mu}}\right)\frac{r}{\sqrt{t}}drdt \qquad (7)$$

Note that $\pi R_{\mathrm{por}}^2\ \rho_{\mathrm{por}}^*$ is the surface porosity.

In a powder bed where flow paths are interconnected, R_{por} is dependent on the particle size and bed porosity, ε. To make Eq. 7 applicable to powder beds, the surface porosity is replaced by ε and the corresponding R_{por} calculated. Integrating Eq. 7 gives:

$$V_{\mathrm{pen}} = \left(\varepsilon\pi\sqrt{\frac{\sigma\cos\theta R_{\mathrm{por}}}{2\mu}}\right)\int_0^{\tau}\frac{r(t)^2}{\sqrt{t}}dt \qquad (8)$$

The value of the integral in Eq. 8 depends on the contact area between the liquid and the powder bed and the duration of that contact. In this work, we define the moment of impact ($t = 0$) as the instant when the drop makes first contact with the powder bed surface. This means that at $t = 0$, $r = 0$.

Currently, we are incapable of predicting the impact behavior of liquid in a powder bed as we do not know how r changes with time, or what its upper limit is. We therefore rely on experimental data, as discussed below.

In Figure 6, we showed the temporal change of the spreading drop diameter in dimensionless form (i.e., D_{b}/D_0 V_{S} t). We have assumed the spreading profile to be hemispherical so we set $D_{\mathrm{b}}(t) = 2{\cdot}r(t)$. Then, the integral in Eq. 8 can be discretized using the trapezoid rule:

$$\int_0^{\tau}\frac{r(t)^2}{\sqrt{t}}dt = \frac{D_0^2}{4}\sum_{i=1}^{N}\frac{1}{2}\left(\frac{(D_{\mathrm{b}}/D_0)_i^2}{\sqrt{t_i}} + \frac{(D_{\mathrm{b}}/D_0)_{i-1}^2}{\sqrt{t_{i-1}}}\right)\Delta t \qquad (9)$$

where $i = 0$ is at $t = 0$ and $i = N$ is at the last t value in each plot. At $t = 0$, $(D_{\mathrm{b}}/D_0)^2/\sqrt{t}$ is assumed to be 0 for all cases. V_{pen} can now be calculated using liquid properties from Table 1 and ε and R_{por} values discussed in the Experimental Setup section. Results are summarized in Table 2.

When model D_{nuc} are compared with experimental data, agreement is within 1.5% for all 60% glycerin, 85% glycerin, and 95% glycerin cases considered here. In addition, predicted values fall within experimental uncertainty for all cases but one. Considering that no fitting parameters were used in the model, and that the model accurately predicts the effect of small differences in spreading behavior on nucleus size, the overall capability of the model is deemed satisfactory. The fact that Eq. 8 yields accurate results implies that drop spreading is an important factor in determining both the rate of nucleation and nuclei sizes.

Table 2. Summary of Nucleation Model Input Parameters and Results

Symbols in Figure 6	◇	◈	◆	△	▲	▽
ε	0.44	0.44	0.44	0.44	0.44	0.44
$\sigma_0 \times 10^3$ (kg/s^2)	63.4	63.4	63.4	65.6	65.6	64.7
$\mu_0 \times 10^3$ (kg/m s)	13	13	13	125	125	544
θ (°)	22.3	22.3	22.3	21.5	21.5	31.0
$R_{\mathrm{p}} \times 10^6$ m (from Eq. 2)	55.8	55.8	55.8	55.8	55.8	55.8
$\int_0^{\tau}\frac{r^2}{\sqrt{t}}dt \times 10^7$, m^{2}s$^{0.5}$ (from Eq. 9 and Fig. 6)	2.58	2.33	2.18	1.69	1.56	1.49
$D_{\mathrm{n}} \times 10^3$, m (model)	2.73	2.69	2.66	2.49	2.46	2.46
$D_{\mathrm{n}} \times 10^3$, m (measured)	2.72 ± 0.07	2.66 ± 0.07	2.62 ± 0.03	2.48 ± 0.07	2.44 ± 0.03	2.44 ± 0.04

Conclusions

The influence of impact conditions on nucleation was studied for single drops impacting a glass bead bed. High speed images of drop impact helped identify the mechanistic steps of nucleation. Results showed that nucleation rate is not influenced by liquid properties for drops spreading significantly after impact (i.e., $30 \leq We \leq 233$). They also showed that nucleus size is determined by how much liquid penetrates into the powder bed during the drop spreading phase, which typically lasted less than 2 ms. Therefore, liquid properties are important in determining nucleus size.

The corresponding analytical model that was developed accurately predicts the nucleus size (to within 1.5%) using only liquid and powder bed properties and the experimentally measured spreading behavior of the drop. It is the first of its kind to predict a nucleus property from general principles and without using any empirical constants. Since, the model currently requires experimental data for the spreading behavior of the drop on a powder bed further research on drop spreading on a powder bed is warranted.

Literature Cited

1. Ennis BJ, Litster JD. *Particle size enlargement*. In: Perry R, Green D, editor. *Perry's Chemical Engineers Handbook*, 7th ed. New York: McGraw-Hill, 1997:56–89.
2. Iveson SM, Litster JD, Hapgood KP, Ennis BJ. Nucleation, growth and breakage phenomena in agitated wet granulation processes: a review. *Powder Technol*. 2001;117:3–39.
3. Agland S, Iveson SM. The impact of liquid drops on powder bed surfaces. CHEMECA '99, The 27th Australasian Chemical Engineering Conference, 26–29 September 1999, Newcastle, Australia, The Institution of Engineers, Australia.
4. Hapgood KP. Nucleation and binder dispersion in wet granulation, PhD thesis. Brisbane, Australia: University of Queensland, 2000.
5. Eshtiaghi N, Liu JS, Shen W, Hapgood KP. Liquid marble formation: spreading coefficients or kinetic energy? *Powder Technol*. 2009;196:126–132.
6. Vonk P, Guillaume CPF, Ramaker JS, Vromans H, Kossen NWF. Growth mechanisms of high-shear pelletisation. *Int J Pharm*. 1997;157:93–102.
7. Schaafsma SH, Vonk P, Segers P, Kossen NWF. Description of agglomerate growth. *Powder Technol*. 1998;97:183–190.
8. Waldie B. Growth mechanism and the dependence of granule size on drop size in fluidized-bed granulation. *Chem Eng Sci*. 1991; 46:2781–2785.
9. Litster JD, Hapgood KP, Michaels JN, Sims A, Roberts M, Kameneni SK, Hsu T. Liquid distribution in wet granulation: dimensionless spray flux. *Powder Technol*. 2001;114:32–49.
10. Hapgood KP, Litster JD, Smith R. Nucleation regime map for liquid bound granules. *AIChE J*. 2003;49:350–361.
11. Knight PC. An investigation of the kinetics of granulation using a high shear mixer. *Powder Technol*. 1993;77:159–169.
12. van den Dries K, Vromans H. Qualitative proof of liquid dispersion and penetration-involved granule formation in a high shear mixer. *Eur J Pharm Biopharm*. 2004;58:551–559.
13. Wildeboer WJ, Koppendraaier E, Litster JD, Howes T, Meesters G. A novel nucleation apparatus for regime separated granulation. *Powder Technol*. 2007;171:96–105.
14. Hapgood KP, Litster JD, Biggs SR, Howes T. Drop penetration into porous powder beds. *J Colloid Interf Sci*. 2002;253:353–366.
15. Denesuk M, Smith GL, Zelinski BJJ, Kreidl NJ, Uhlmann DR. Capillary penetration of liquid droplets into porous materials. *J Colloid Interf Sci*. 1993;158:114–120.
16. Middleman S. *Modeling Axisymmetric Flows: Dynamics of Films, Jets, and Drops*. San Diego: Academic Press, 1995.
17. Fox RW, Pritchard PJ, McDonald AT. *Introduction to Fluid Mechanics*, 7th ed. New York: Wiley, 2009.
18. Schaefer T, Mathiesen C. Melt pelletization in a high-shear mixer: IX. Effects of binder particle size. *Int J Pharm*. 1996;139:139–148.
19. Washburn EW. The dynamics of capillary flow. *Phys Rev*. 1921; 17:273–283.

Manuscript received May 25, 2010, revision received Sept. 30, 2010, and final revision received Jan. 14, 2011.